Chinese Chemical Letters 34 (2023) 107511

Contents lists available at ScienceDirect

Chinese Chemical Letters

journal homepage: www.elsevier.com/locate/cclet

Construction of FRET-based metallacycles with efficient photosensitization efficiency and photocatalytic activity

Peipei Jia[a], Yixiong Hu[a], Zhiyong Zeng[a], Yute Wang[a], Bo Song[a], Yanrong Jiang[b], Haitao Sun[b], Ming Wang[a], Wenwei Qiu[a,*], Lin Xu[a,c,*]

[a] Shanghai Key Laboratory of Green Chemistry and Chemical Processes, Shanghai Frontiers Science Center of Molecule Intelligent Syntheses, Shanghai Engineering Research Center of Molecular Therapeutics and New Drug Development, School of Chemistry and Molecular Engineering, East China Normal University, Shanghai 200062, China
[b] State Key Laboratory of Precision Spectroscopy, East China Normal University, Shanghai 200241, China
[c] Institute of Eco-Chongming, Shanghai 202162, China

ARTICLE INFO

Article history:
Received 24 December 2021
Revised 8 May 2022
Accepted 10 May 2022
Available online 16 May 2022

Keywords:
Self-assembly
Metallacycle
FRET
Photosensitization
Photocatalytic

ABSTRACT

The fabrication of highly effective photosensitizers has received considerable attention because of their attractive functions and applications in the fields of photodynamic therapy, photosynthesis, photocatalysis, *etc*. Thus, it is highly desirable to develop a new approach to enhance photosensitization efficiency. Herein, through coordination-driven self-assembly, a series of metallacycles with efficient fluorescence resonance energy transfer (FRET) were effectively constructed, which displayed higher photosensitization efficiency and photocatalytic activity than their model metallacycles without FRET due to broadband absorption and singlet energy transfer from the energy acceptor to the energy donor. Moreover, iodization of fluorophores induced a significant enhancement of the photosensitization efficiency and photocatalytic activity of the metallacycles. This research provides an efficient strategy for improving photosensitization efficiency and a promising platform for the preparation of effective photosensitizers and photocatalysts.

During recent decades, the development of new photosensitizers has attracted much attention due to their wide application in the fields of photodynamic therapy [1–4], photosensitive catalysis [5–9] and 3D printing [10,11]. Photosensitization efficiency is an important parameter to evaluate the performance of photosensitizers; thus, improving photosensitization efficiency is a long-term pursuit in this field [12–15]. In the photosensitization process, increasing the spin-orbit coupling (SOC) constant or decreasing the energy level difference between the single and triple excited states (ΔE_{ST}) can increase the intersystem crossing (ISC) rate to improve the photosensitization efficiency [16]. At present, introducing multiple heavy atoms (Br, I, Pt, *etc*.) to promote spin-orbit coupling is a common method to improve photosensitization efficiency [17,18]. Incorporating a π-conjugated system into photosensitizer molecules through covalent organic synthesis to reduce the energy level difference (ΔE_{ST}) of S_1 to T_1 through separation of the frontier molecular orbital between the HOMO and LUMO is another effective strategy [19,20]. For example, Liu and co-workers demonstrated polymerization-enhanced photosensitization, which promotes the transition of the photosensitizer from S_1 to T_1 and can improve its light absorption capacity for higher photosensitization efficiency than the small-molecule analogues [21]. Therefore, the development of a new approach to enhance photosensitization efficiency is of great value.

At present, most reported photosensitizers are based on a unichromophore profile, in which UV-vis absorption covers only a small major absorption band in the visible spectrum, which is detrimental to the application of photosensitizers, especially with broadband excitation light source such as solar light [22,23]. However, FRET systems containing at least two kinds of chromophores (named energy donors and energy acceptors, respectively) show broadband absorption in the visible spectrum since both the energy donors and the energy acceptors exhibit strong absorption in the visible spectral region with different wavelengths [24–30]. Therefore, FRET was used to enhance light absorption by accessing strong and broadband absorption in the visible region [31–36]. As shown in Fig. 1, in FRET systems, both the energy donor and the

* Corresponding authors at: Shanghai Key Laboratory of Green Chemistry and Chemical Processes, Shanghai Frontiers Science Center of Molecule Intelligent Syntheses, Shanghai Engineering Research Center of Molecular Therapeutics and New Drug Development, School of Chemistry and Molecular Engineering, East China Normal University, Shanghai 200062, China.

E-mail addresses: wwqiu@chem.ecnu.edu.cn (W. Qiu), lxu@chem.ecnu.edu.cn (L. Xu).

https://doi.org/10.1016/j.cclet.2022.05.025
1001-8417/

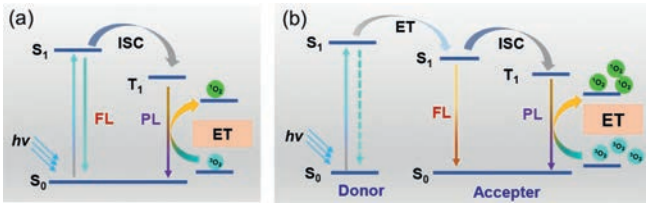

Fig. 1. Mechanism of a unichromophore photosensitizer (a) and a multichromophore photosensitizer with FRET (b).

energy acceptor can be excited upon irradiation with visible light as well as singlet energy transfer from the energy donor to the energy acceptor, producing the triplet excited state in turn, which induces higher photosensitization efficiency compared to that of reference photosensitizers that are based on a unichromophore profile. Thus, we envision that the construction of photosensitizers with FRET might be an effective approach to improving the efficiency of photosensitization.

Coordination-driven self-assembly, based on metal-ligand coordination interactions, has been proven to be an efficient strategy to construct functionalized discrete 2D metallacycles and 3D metallacages [37–48]. This strategy provides considerable synthetic advantages, such as few steps and fast and facile preparation of the final products. More importantly, the coordination-driven self-assembly strategy allows precise control over the shape and size of the final assemblies as well as the distribution and total number of incorporated functional moieties [49–57]. For example, recently, we effectively constructed a FRET-based metallacycle through a coordination-driven self-assembly strategy with coumarin and rhodamine as the energy donor and the energy acceptor, respectively, which presented the first successful example of real-time monitoring of the process and dynamics of coordination-driven self-assembly [58]. Therefore, coordination-driven self-assembly is a very efficient method of preparing FRET systems.

Based on the consideration that introducing both heavy atoms and the FRET process could enhance the photosensitization efficiency, in this study, we constructed a FRET-based hexagonal metallacycle **M1** through coordination-driven self-assembly (Scheme 1). For **M1**, coumarin chromophore was selected as the energy donor, and diiodo-BODIPY chromophore was selected not only as the energy acceptor but also as the photosensitive unit. To explore the effect of introducing iodine atoms on the photosensitivity efficiency, FRET-based model metallacycle **M2** functionalized with coumarin and BODIPY chromophores was designed and prepared. Additionally, in order to investigate the effect of the FRET process on the photosensitivity efficiency and to determine the Förster energy transfer efficiency, a series of model metallacycles **M3**, **M4**, and **M5** functionalized with diiodo-BODIPY, BODIPY, or coumarin chromophore were also prepared. As expected, compared with the model metallacycles **M3** and **M4** containing only the terminal acceptor (diiodo-BODIPY or BODIPY chromophore), the FRET-based metallacycles **M1** and **M2** with broad absorption bands in the visible region showed higher photosensitization efficiency and photocatalytic photooxidation activity, respectively. Moreover, metallacycles **M1** and **M3** with diiodo-BODIPY chromophore displayed higher photosensitization efficiency and photocatalytic activity than the corresponding metallacycles **M2** and **M4** with BODIPY chromophore, respectively. The results indicated that the introduction of both heavy atoms and the FRET process are efficient strategies for enhancing the photosensitization efficiency of photosensitizers.

The 120° diiodo-BODIPY-containing diplatinum(II) building block **L1** and BODIPY-containing diplatinum(II) building block **L2**, chosen as the energy acceptors and photosensitive units, were designed and synthesised through an esterification reaction, as presented in the Supporting Information (Scheme 1 and Schemes S1-S4 and Figs. S1-S12 in Supporting information). The 120º dipyridyl building block **L3**, labelled with coumarin as an energy donor, was designed and synthesised according to the reported methods. Moreover, with the aim of investigating the energy transfer efficiencies, model building blocks **L4** and **L5** without any chromophore were also designed and synthesised through an esterification reaction (Scheme 1 and Schemes S5-S7 in Supporting information).

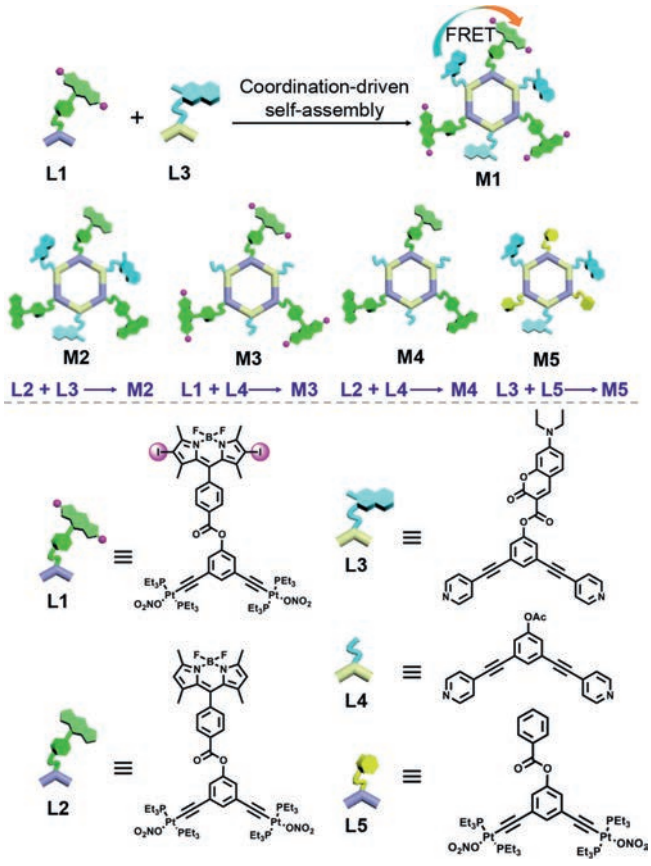

Scheme 1. Schematic illustration of the coordination-driven self-assembly of hexagonal metallacycles **M1**-**M5** and the chemical structures of building blocks **L1**-**L5**.

According to the design principles of coordination-driven self-assembly, the self-assembly of three 120° donor ligands and three 120° acceptor ligands can produce a discrete hexagonal metallacycle [57,58]. By stirring a mixture of 120° acceptor ligand **L1** and 120° donor ligand **L3** in a stoichiometric ratio in acetone/water (5/1, v/v) at 50 °C, the pivotal hexagonal metallacycle **M1** was obtained in almost quantitative yield (Scheme 1 and Scheme S8 in Supporting information). Furthermore, the model metallacycles **M2**-**M5** were prepared through the coordination-driven self-assembly of ligands **L1**-**L5** (Scheme 1 and Schemes S9-S14 in Supporting information). The formation of hexagonal metallacycles **M1**-**M5** with a discrete and highly symmetric scaffold was supported by multinuclear NMR spectroscopy (^{1}H, ^{31}P{^{1}H}, ^{13}C, 2D DOSY, ^{1}H-^{1}H COSY, ^{1}H-^{1}H NOESY) (Figs. S13-S45 in Supporting information). All ^{31}P{^{1}H} NMR spectra of **M1**-**M5** showed a sharp singlet, which shifted upfield from the starting di-Pt(II) acceptors. For instance, in the ^{1}H NMR spectrum, the peaks of α- and β-hydrogen of **M1** showed downfield shifts (for α-H, $\Delta\delta\approx$0.39 ppm; for β-H, $\Delta\delta\approx$0.41 ppm) compared with 120° monodipyridyl donor **L3**, which was associated with the formation of Pt-N bonds (Figs.

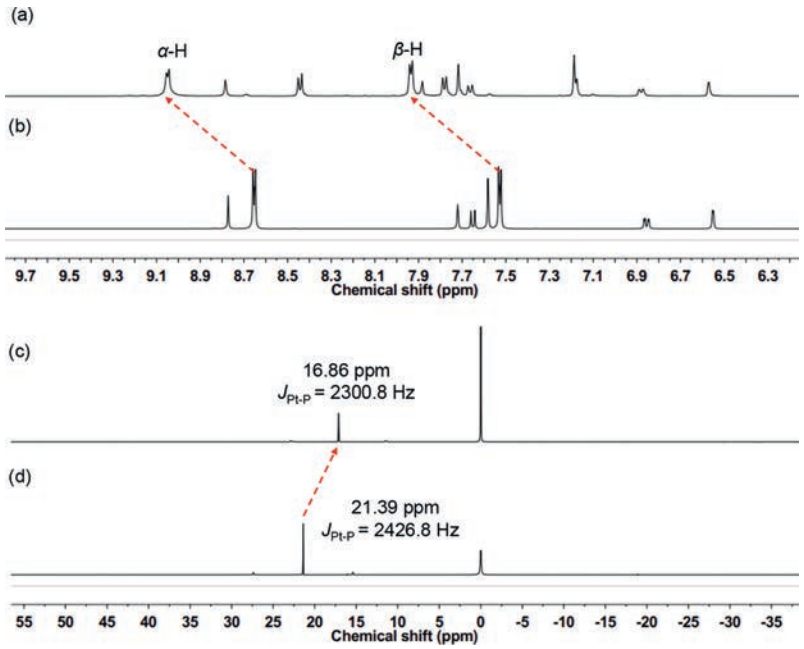

Fig. 2. Partial ^{1}H NMR spectra (500 MHz, acetone-d_6, 298 K) of metallacycle **M1** (a) and 120° dipyridyl donor **L3** (b). ^{31}P NMR spectra (202 MHz, acetone-d_6, 298 K) of metallacycle **M1** (c) and 120° diplatinum(II) acceptor **L1** (d).

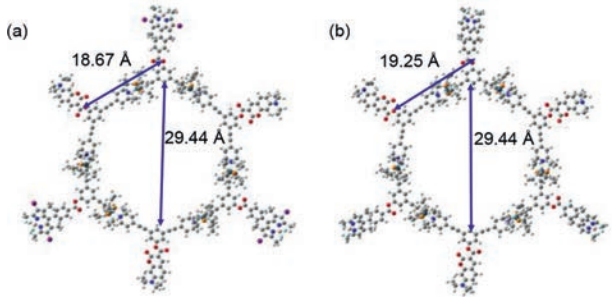

Fig. 3. Simulated geometric structures of metallacycles **M1** (a), **M2** (b).

2a and b). Moreover, **M1** displayed a sharp singlet at 16.86 ppm, shifted upfield by approximately 4.53 ppm compared with the corresponding starting acceptor **L1** singlet. The upfield shift, as well as the decrease of coupling of the flanking ^{195}Pt satellites (*e.g.*, *ca.* $\Delta J_{P-Pt} = -126.0$ Hz for **M1**), was attributed to electron back-donation from the platinum atoms (Figs. 2c and d). Furthermore, the characterization by 2D ^{1}H NMR techniques is consistent with the structure of discrete metallacycles. For example, cross-peaks between the signals of PEt_3 protons (CH_2 and CH_3) and pyridine protons (α- and β-hydrogen) appeared in 2D ^{1}H-^{1}H NOESY. The signals supported the structure of metallacycles based on the formation of Pt-N bonds. In addition, the observation of a single band in 2D DOSY supported the formation of isolated species.

All attempts to grow X-ray-quality single crystals of hexagonal metallacycles **M1-M5** proved unsuccessful. The GFN2-xTB (geometry, frequency, noncovalent, extended tight binding) semiempirical tight-binding method was employed to acquire further insight into the structural characteristics of these metallacycles. Molecular simulation indicated that metallacycles **M1**-**M5** all featured a very similar and roughly planar hexagonal ring with an internal diameter of approximately 3.0 nm (Fig. 3 and Fig. S46 in Supporting infortion). Moreover, the coumarin units and BODIPY units in metallacycle **M1** were close to each other at a distance of approximately 1.9 nm, which fully satisfies the requirements of FRET for the distance (<10 nm) between the donor and the receptor fluorophores (Fig. 3).

BODIPY is a versatile chromophore with numerous advantageous properties, such as strong absorption of visible light, easy functionalization, and excellent photostability [59–61]. To date, BODIPY/diiodo-BODIPY dyes have been widely used in the fields of photodynamic therapy, light harvesting, bioimaging, fluorescent probes, *etc.* [62–65]. In this study, coumarin and BODIPY/diiodo-BODIPY were selected as the FRET donor and acceptor fluorophores, respectively, because the emission spectrum of coumarin and the absorption spectrum of BODIPY/diiodo-BODIPY have a large overlap, which is beneficial for FRET. To investigate the energy transfer from coumarin to BODIPY/diiodo-BODIPY, the absorption and emission spectra of these ligands and metallacycles were measured (Fig. 4, Table S1, Figs. S47 and S48 in Supporting infortion). The ligands **L1** and **L2** gave maximum absorption at 534 nm and 500 nm, respectively. However, ligand **L1** showed weaker orange emission at 562 nm than **L2** displaying bright green emission at 520 nm, which was attributed to the heavy atom effects resulting in absorption and emission redshifts and fluorescence quenching. The energy donor **L3** had maximum absorption at 427 nm and blue emission at 468 nm. As shown in Figs. 4a and e, the normalized absorption spectra of **L1** and **L2** overlapped with the emission spectrum of **L3**, which was favourable for FRET within metallacycles **M1** and **M2**. Likewise, the normalized absorption spectra of metallacycles **M3** and **M4** displayed overlap with the emission spectrum of **M5** (Figs. 4b and f). However, the overlap between **M4** and **M5** was greater than that between **M3** and **M5**, which is attributed to the absorption redshift of 34 nm caused by the introduction of iodine atoms into **M3**.

Moreover, when excited at the optimal wavelength for coumarin, metallacycle **M1** showed stronger emission at 562 nm than metallacycle **M3** and weaker emission at 469 nm than the coumarin-modified metallacycle **M5** (Fig. 4c). Similarly, metallacycle **M2** showed stronger emission at 522 nm than metallacycle **M4** and weaker emission at 469 nm than metallacycle **M5** (Fig. 4g), which all indicated a typical FRET process that generally causes a decrease in the donor emission and an increase in the accepter

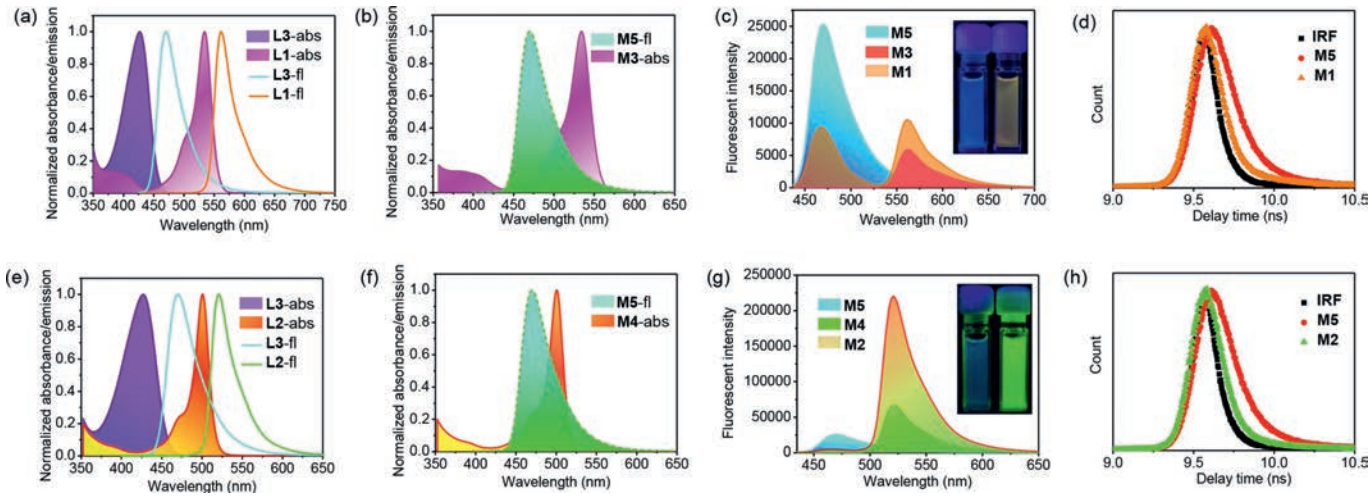

Fig. 4. (a) Normalized emission spectra of ligands **L1** and **L3** (30 μmol/L) and absorption spectra of **L1** and **L3** (30 μmol/L). (b) Normalized emission spectrum of **M5** (10 μmol/L) and absorption spectrum of **M3** (10 μmol/L). (c) Fluorescence emission spectra of metallacycles **M1**, **M3** and **M5** (10 μmol/L). (d) Fluorescence lifetimes of **M5** and **M1** upon excitation at 427 nm (10 μmol/L). (e) Normalized emission spectra of ligands **L2** and **L3** (30 μmol/L) and absorption spectra of **L2** and **L3** (30 μmol/L). (f) Normalized emission spectrum of **M5** (10 μmol/L) and absorption spectrum of **M4** (10 μmol/L). (g) Fluorescence emission spectra of metallacycles **M2**, **M4** and **M5** (10 μmol/L) in acetone. (h) Fluorescence lifetimes of **M5** and **M2** upon excitation at 427 nm (10 μmol/L) ($\lambda_{ex} = 427$ nm; slit (5, 5)).

emission. Based on the ratio between the fluorescence intensities of the donor (coumarin) in the absence (for metallacycle **M5**) and presence (for metallacycles **M1** and **M2**) of the acceptor (BODIPY), the energy transfer efficiency (Φ_{ET}) from coumarin to BODIPY in metallacycles **M1** and **M2** was calculated to be 60.9% and 80.1%, respectively. Metallacycle **M1** showed a lower Φ_{ET} than metallacycle **M2,** which was attributed to the redshifted absorption spectrum of **L1** decreasing the overlap between the emission spectrum of energy donor and the absorption spectrum of energy acceptor. Moreover, the fluorescence lifetime of metallacycle **M1** (0.11 ns) or **M2** (0.07 ns) was shorter than that of metallacycle **M5** (0.27 ns), which strongly supported the existence of the energy transfer process from coumarin to diiodo-BODIPY/BODIPY in metallacycles **M1** and **M2** (Figs. 4d and h) [66].

During the past several decades, $^1O_2$ has been widely applied in photodynamic therapy (PDT), photochemistry, and catalysis [67,68]. Moreover, as a photosensitizer, BODIPY is able to produce singlet oxygen ($^1O_2$) for photocatalysis and PDT [69,70]. As one of the most important parameters of photosensitizers, the $^1O_2$ generation efficiencies of **M1-M4** were determined to evaluate their photosensitization efficiencies. Herein, 9,10-dimethylanthracene (DMA), which can react with $^1O_2$ to form endoperoxide and thereby decrease its emission, was used to evaluate the $^1O_2$ generation ability of metallacycles **M1-M4** (Fig. 5). As shown in Fig. S49 (Supporting information), the fluorescence emission of DMA at 400-500 nm decreased rapidly upon photoirradiation, confirming the successful generation of $^1O_2$ by the photosensitizer. The $^1O_2$ generation rate can be quantitatively evaluated by plotting $\ln(A_0/A_t)$ against the irradiation time (Figs. 5a and b, Table S2 in Supporting information). It is worth noting that the singlet oxygen generation rates of ligands **L1** and **L2** were almost the same as that of the metallacycles **M3** and **M4**, which showed that the formation of metallacycles did not affect singlet oxygen capacity of the ligands. Due to the absence of photosensitive unit diiodo-BODIPY/BODIPY, **L3** and **M5** did not have the ability to produce singlet oxygen (Fig. 5c). According to the data fitting results, the singlet oxygen generation rates of metal lacycles **M1-M4** were 9.48 min^{-1}, 0.30 min^{-1}, 5.04 min^{-1}, and 0.16 min^{-1}, respectively (Fig. 5d). The relative changes in the DMA fluorescence intensity of metallacycle **M1** exhibited the highest $^1O_2$ generation ability compared with any other metallacycle, approximately 31.6-fold, 1.88-fold and 59.2-fold higher than those

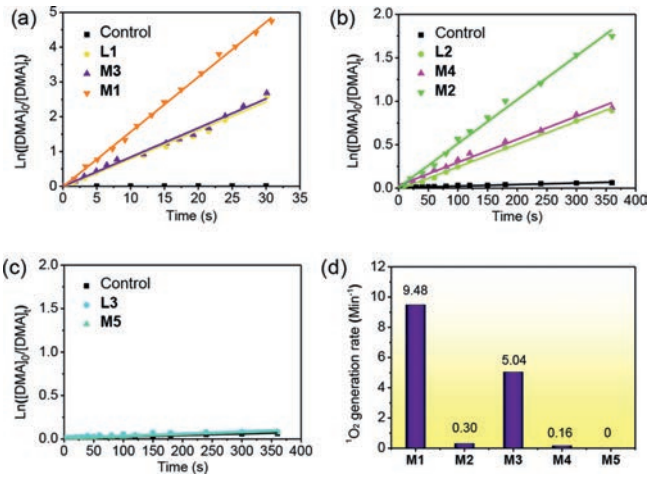

Fig. 5. The decomposition of DMA by (a) **L1**, **M3**, **M1**, (b) **L2**, **M4**, **M2**, (c) **L3**, **M5** in acetone. (d) The histogram of $^1O_2$ generation rate of **M1**-**M4**.

of **M2**, **M3** and **M4**, respectively. Notably, due to the introduction of heavy atoms (iodine atoms) to enhance the spin-orbit coupling of the photosensitizer, the relative changes in the DMA fluorescence intensity of **M1** and **M3** were both higher than those of **M2** and **M4**, respectively. Additionally, FRET-based metallacycles **M1** and **M2** were more efficient than unichromophore-based metallacycles **M3** and **M4** for the photooxidation of DMA, respectively. For instance, the singlet oxygen generation efficiency of metallacycle **M1** was nearly twice that of metallacycle **M3**. That was because the occurrence of the FRET process resulting in broadband absorption in the visible region enhanced the photosensitization ability of the photosensitizers. Thus, FRET process in combination with heavy atom effect could increase the photosensitization ability of the photosensitizer, although heavy atom effect plays more pivotal role in $^1O_2$ generation than FRET in these cases.

According to previous studies, BODIPY dyes can generate $^1O_2$ for the photooxidation of sulphides [71,72]. To demonstrate the utility of the photosensitizer, we employed a simple 2-chloroethyl methyl sulfide (CEES, a chemical warfare agent simulant of mustard gas) as a model substrate to evaluate the oxidative catalytic

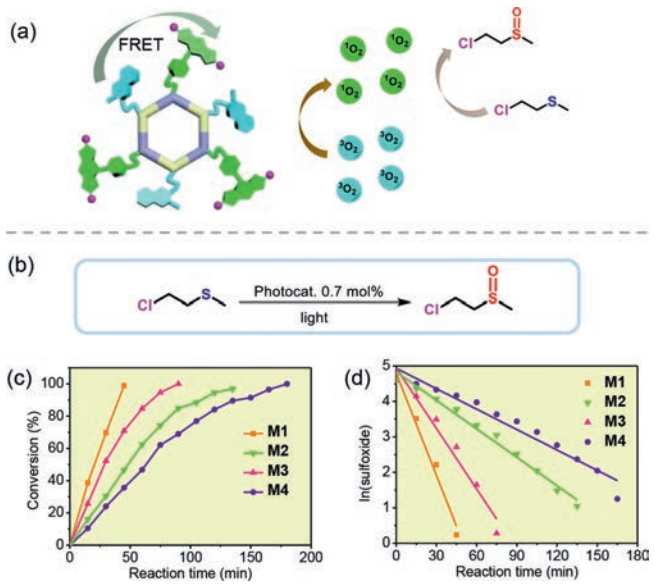

Fig. 6. (a) Generation of singlet oxygen ($^1O_2$) and the photooxidation reaction of **M1**. (b) Photooxidation of sulfides from CEES to CEESO. (c) Kinetic plot of the photooxidation of sulfides catalysed by **M1-M4** under irradiation. (d) Calculation of the pseudo-first-order kinetic rate constant, *k*, from the slope of the ln[sulfoxide] *vs.* time plot, where [sulfoxide] = 100 − (sulfide conversion).

activity of metallacycle **M1** (Fig. 6). For comparison, oxidative catalytic activities of metallacycles **M2**, **M3**, and **M4** were also investigated. Since the singlet oxygen generation rates of ligands **L1** and **L2** were almost the same as that of the metallacycles **M3** and **M4**, respectively, oxidative catalytic activities of metallacycles ligands **L1** and **L2** were not conducted. Moreover, due to the absence of photosensitive unit diiodo-BODIPY/BODIPY, **L3** and **M5** did not have the ability to produce singlet oxygen (Fig. 5c), the photocatalytic activity of **L3** and **M5** were not investigated yet. The components of the reaction systems were identified and quantified through gas chromatography-mass spectrometer (GC-MS) analysis. The results showed that all metallacycles **M1**-**M4** could effectively catalyze the oxidation of sulfide with outstanding conversion rates while metallacycle **M1** displayed the best catalytic performance (Fig. 6c). For instance, full conversion from CEES to monooxygenated-sulfoxide (CEESO) but not to the toxic sulfone ($CEESO_2$) catalyzed by metallacycle **M1** was observed after 45 min of 6 W white LED irradiation. With the same reaction conditions, metallacycles **M2**, **M3**, and **M4** exhibited 47%, 71% and 35% conversion, respectively, after 45 min of reaction. The turnover frequency (TOF) of **M1-M4** was calculated to 80.78 h^{-1}, 23.66 h^{-1}, 47.74 h^{-1}, 16.10 h^{-1}, respectively (Fig. 6d and Table S3 in Supporting information). The results indicated that the introduction of the heavy atoms as well as FRET system were effective methods for improving photocatalytic efficiency.

To study the adaptability of the photosensitizer to the substrate, the photocatalytic oxidation activity of the thioether derivatives was also studied (Table 1 and Figs. S50-S64 in Supporting information). Considering that metallacycle **M1** has the best catalytic performance, metallacycle **M1** was chosen as catalyst to catalyze the oxidation of sulfide compounds with different substituents and steric hindrance, the results showed that the catalytic effect of mono-substituted methyl phenyl sulfide was not particularly affected by the introduction of electron-donating group or electron-withdrawing group with low steric hindrance (Table 1, entries 1-7). However, with the introduction of conjugated substituents, such as diphenylthioether, the catalytic effect was sharply reduced, and the catalytic efficiency was not significantly improved by prolonging

Table 1
Results of selective oxidation of various sulfides catalysed by **M1**.

Entry	Substrate	Product	Reaction time (h)	Con (%)
1	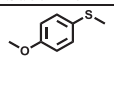	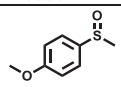	3	> 99
2	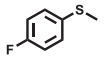	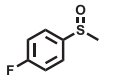	4	> 99
3	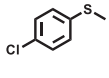	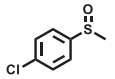	3	> 99
4	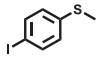	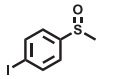	4	> 99
5	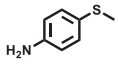	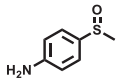	6	> 99
6	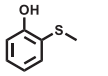	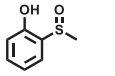	4	> 99
7	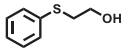	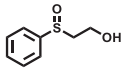	4	> 99
8	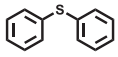	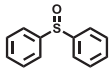	6	43
9	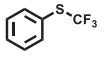	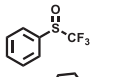	6	0
10			6	0
11	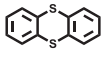	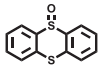	6	29
12			4	> 99
13	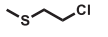	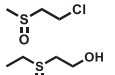	3	> 99
14	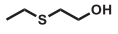	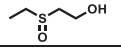	2	> 99

The experimental conditions were as follows: substrate (0.1 mmol), catalyst (0.7 mol%), internal standard (0.1 mmol of dodecane) and solvent (methanol/acetone, 2/1, 1.5 mL), the conversion of the reaction were determined by GC-MS.

the reaction time (Table 1, entry 8). Phenyl(trifluoromethyl)sulfide, with a strong electron-withdrawing group, did not produce the corresponding sulfoxide products (Table 1, entry 9). The oxygenation of dibenzo[b,d]thiophene could not be realized under our catalytic conditions since the conjugation effect reduces the electron cloud density of sulfur (Table 1, entry 10). Thianthrene was proved to be inferior for this oxygenation due to the formation of by-products (Table 1, entry 11). It is gratifying that phenoxathiine and alkyl sulfides were compatible with our oxidation system, even with sensitive groups (Table 1, entries 12-14). From the above data, it could be seen that a relatively efficient photooxidation of sulfides was achieved in most cases, demonstrating the general applicability of metallacycle **M1** as a highly efficient photocatalyst.

In summary, we have developed a strategy to utilize FRET and heavy atom effects simultaneously to improve the photosensitization efficiency and photocatalytic activity of photosensitizers. Through coordination-driven self-assembly, the discrete and highly symmetric hexagonal metallacycle **M1** bearing precise numbers of coumarin and diiodo-BODIPY moieties was effectively constructed. In comparison with the unichromophore-based metallacycles **M3** and **M4**, the FRET-based metallacycles **M1** and **M2** displayed higher photosensitization efficiency for generating $^1O_2$ and photocatalytic activity for the photooxidation of sulfides. Moreover,

metallacycles **M1** and **M3** with iodination showed higher photosensitive efficiency and photocatalytic activity than metallacycles **M2** and **M4** without iodination, respectively. This study demonstrates a successful strategy for improving photosensitization efficiency and photocatalytic activity. Furthermore, this research provides a prospective platform for designing efficient photosensitizers and for the application of these compounds in photocatalysis.

Declaration of competing interest

The authors declare that they have no known competing financial interests or personal relationships that could have appeared to influence the work reported in this paper.

Acknowledgments

This work was supported by the National Nature Science Foundation of China (No. 21871092), Program of Shanghai Outstanding Academic Leaders (No. 21XD1421200), the Fundamental Research Funds for the Central Universities, and 2021 Academic Innovation Ability Enhancement Plan for Excellent Doctoral Students of East China Normal University (No. YBNLTS2021-025).

Supplementary materials

Supplementary material associated with this article can be found, in the online version, at doi:10.1016/j.cclet.2022.05.025.

References

[1] V.N. Nguyen, Y. Yan, J. Zhao, J. Yoon, Acc. Chem. Res. 54 (2021) 207–220.
[2] Y. Qin, L.J. Chen, F. Dong, et al., J. Am. Chem. Soc. 141 (2019) 8943–8950.
[3] B. Huang, X. Liu, G. Yang, et al., CCS Chem. 2 (2021) 2055–2066.
[4] H. Zhu, Q. Li, B. Shi, et al., Angew. Chem. Int. Ed. 59 (2020) 20208–20214.
[5] L. Zeng, T. Liu, C. He, et al., J. Am. Chem. Soc. 138 (2016) 3958–3961.
[6] J. Guo, Y.Z. Fan, Y.L. Lu, S.P. Zheng, C.Y. Su, Angew. Chem. Int. Ed. 59 (2020) 8661–8669.
[7] L.J. Chen, S. Chen, Y. Qin, et al., J. Am. Chem. Soc. 140 (2018) 5049–5052.
[8] J. Zhu, X. Liu, J. Huang, L. Xu, Chin. Chem. Lett. 30 (2019) 1767–1774.
[9] Z. Zhang, Z. Zhao, Y. Hou, et al., Angew. Chem. Int. Ed. 58 (2019) 8862–8866.
[10] M. Gastaldi, F. Cardano, M. Zanetti, et al., ACS Mater. Lett. 3 (2021) 1–17.
[11] S.R. Martínez, Y.B. Palacios, D.A. Heredia, et al., ACS Appl. Mater. Interfaces 13 (2021) 11597–11608.
[12] H.Y. Lin, L.Y. Zhou, L. Xu, Chem. Asian J. 16 (2021) 3805–3816.
[13] S. Xu, W. Wu, X. Cai, et al., Chem. Commun. 53 (2017) 8727–8730.
[14] Y.X. Hu, W.J. Li, P.P. Jia, et al., Adv. Opt. Mater. (2020) 2000265.
[15] W. Zhao, Z. He, Q. Peng, et al., Nat. Commun. 9 (2018) 3044.
[16] K. Schmidt, S. Brovelli, V. Coropceanu, et al., J. Phys. Chem. A 111 (2007) 10490–10499.
[17] W.J. Li, Z. Hu, L. Xu, et al., J. Am. Chem. Soc. 142 (2020) 16748–16756.
[18] J. Zou, Z. Yin, K. Ding, et al., ACS Appl. Mater. Interfaces 9 (2017) 32475–32481.
[19] T. Yogo, Y. Urano, Y. Ishitsuka, F. Maniwa, T. Nagano, J. Am. Chem. Soc. 127 (2005) 12162–12163.
[20] R. Acharya, S. Cekli, C.J. Zeman, R.M. Altamimi, K.S. Schanze, J. Phys. Chem. Lett. 7 (2016) 693–697.
[21] W. Wu, D. Mao, S. Xu, et al., Chem. 4 (2018) 1937–1951.
[22] Z. Shi, X. Han, W. Hu, et al., Chem. Soc. Rev. 49 (2020) 7533–7567.
[23] W. Zhou, X. Fang, Q. Qiao, et al., Chin. Chem. Lett. 32 (2021) 943–946.
[24] L. Wu, C. Huang, B.P. Emery, et al., Chem. Soc. Rev. 49 (2020) 5110–5139.
[25] Y. Qin, L.J. Chen, Y. Zhang, et al., Chem. Commun. 55 (2019) 11119–11122.
[26] G. Chen, F. Song, X. Xiong, X. Peng, Ind. Eng. Chem. Res. 52 (2013) 11228–11245.
[27] X. Zhang, L. Wang, N. Li, Y. Xiao, Chin. Chem. Lett. 32 (2021) 2395–2399.
[28] P.P. Jia, L. Xu, Y.X. Hu, et al., J. Am. Chem. Soc. 143 (2021) 399–408.
[29] Z. Guo, J. Zhao, Y. Liu, et al., Chin. Chem. Lett. 32 (2021) 1691–1695.
[30] C. Qin, Y. Li, Q. Li, C. Yan, L. Cao, Chin. Chem. Lett. 32 (2021) 3531–3534.
[31] L. Yuan, W. Lin, K. Zheng, S. Zhu, Acc. Chem. Res. 46 (2013) 1462–1473.
[32] X. Tao, Z. Liao, Y. Zhang, et al., Chin. Chem. Lett. 32 (2021) 791–795.
[33] Q. Ling, T. Cheng, S. Tan, J. Huang, L. Xu, Chin. Chem. Lett. 31 (2020) 2884–2890.
[34] H.Q. Peng, L.Y. Niu, Y.Z. Chen, et al., Chem. Rev. 115 (2015) 7502–7542.
[35] Z. Zhang, Z. Zhao, L. Wu, et al., J. Am. Chem. Soc. 142 (2020) 2592–2600.
[36] Y. Li, Y. Dong, L. Cheng, et al., J. Am. Chem. Soc. 141 (2019) 8412–8415.
[37] M. Tominaga, K. Suzuki, T. Murase, M. Fujita, J. Am. Chem. Soc. 127 (2005) 11950–11951.
[38] T.R. Cook, Y.R. Zheng, P.J. Stang, Chem. Rev. 113 (2013) 734–777.
[39] G.H. Clever, P. Punt, Acc. Chem. Res. 50 (2017) 2233–2243.
[40] Y. Wang, Q. Zhou, X. He, et al., Chin. Chem. Lett. 33 (2022) 1613–1618.
[41] Y.F. Han, G.X. Jin, Acc. Chem. Res. 47 (2014) 3571–3579.
[42] J. Dong, C. Tan, K. Zhang, et al., J. Am. Chem. Soc. 139 (2017) 1554–1564.
[43] J. Zheng, Z. Lu, K. Wu, G.H. Ning, D. Li, Chem. Rev. 120 (2020) 9675–9742.
[44] J. Liu, L. Chen, H. Cui, et al., Chem. Soc. Rev. 43 (2014) 6011–6061.
[45] L. Xu, D. Zhang, T.K. Ronson, J.R. Nitschke, Angew. Chem. Int. Ed. 59 (2020) 7435–7438.
[46] H. Nian, L. Cheng, L. Wang, et al., Angew. Chem. Int. Ed. 60 (2021) 15354–15358.
[47] L.X. Cai, D.N. Yan, P.M. Cheng, et al., J. Am. Chem. Soc. 143 (2021) 2016–2024.
[48] D. Samanta, P.S. Mukherjee, J. Am. Chem. Soc. 136 (2014) 17006–17009.
[49] X. Yan, T.R. Cook, P. Wang, F. Huang, P.J. Stang, Nat. Chem. 7 (2015) 342–348.
[50] C. Mu, Z. Zhang, Y. Hou, et al., Angew. Chem. Int. Ed. 60 (2021) 12293–12297.
[51] Z. Wang, L. He, B. Liu, et al., J. Am. Chem. Soc. 142 (2020) 16409–16419.
[52] J.L. Zhu, L. Xu, Y.Y. Ren, et al., Nat. Commun. 10 (2019) 4285.
[53] X. Liu, Y. Qin, J. Zhu, et al., Chin. Chem. Lett. 32 (2021) 1537–1540.
[54] A. Kumar, R. Saha, P.S. Mukherjee, Chem. Sci. 12 (2021) 5319–5329.
[55] D. Zhang, T.K. Ronson, L. Xu J.R. Nitschke, J. Am. Chem. Soc. 142 (2020) 9152–9157.
[56] M. Yamashina, M.M. Sartin, Y. Sei, et al., J. Am. Chem. Soc. 137 (2015) 9266–9269.
[57] Y.X. Hu, X. Hao, L. Xu, et al., J. Am. Chem. Soc. 142 (2020) 6285–6294.
[58] C.B. Huang, L. Xu, J.L. Zhu, et al., J. Am. Chem. Soc. 137 (2017) 9459–9462.
[59] N. Boens, V. Leena, W. Dehaen, Chem. Soc. Rev. 41 (2012) 1130–1172.
[60] L.Y. Niu, Y.S. Guan, Y.Z. Chen, et al., J. Am. Chem. Soc. 134 (2012) 18928–18931.
[61] Y. Xiao, F. Cai, X. Peng, et al., Chin. Chem. Lett. 32 (2021) 3566–3569.
[62] J. Zhou, Y. Zhang, G. Yu, et al., J. Am. Chem. Soc. 140 (2018) 7730–7736.
[63] C. Li, P.P. Jia, Y.L. Xu, et al., Sci. China Chem. 64 (2021) 134–142.
[64] R. Ziessel, A. Harriman, Chem. Commun. 47 (2011) 611–631.
[65] Y. Qin, X. Liu, P.P. Jia, L. Xu, H.B. Yang, Chem. Soc. Rev. 49 (2020) 5678–5703.
[66] K. Acharyya, S. Bhattacharyya, H. Sepehrpour, et al., J. Am. Chem. Soc. 141 (2019) 14565–14569.
[67] A. Kamkaew, S.H. Lim, H.B. Lee, et al., Chem. Soc. Rev. 42 (2013) 77–88.
[68] L. Cheng, C. Wang, L. Feng, K. Yang, Z. Liu, Chem. Rev. 114 (2014) 10869–10939.
[69] G. Ng, J. Yeow, J. Xu, C. Boyer, Polym. Chem. 8 (2017) 2841–2851.
[70] P. Kluson, M. Drobek, A. Kalaji, et al., Photochem. Photobiol. A 199 (2008) 267–273.
[71] A. Atilgan, M.M. Cetin, J. Yu, et al., J. Am. Chem. Soc. 142 (2020) 18554–18564.
[72] H. Wang, G.W. Wagner, A.X. Lu, et al., ACS Appl. Mater. Interfaces 10 (2018) 18771–18777.